

Electronic Supplemental Information

Unusual aliovalent doping effects on oxygen non-stoichiometry in medium-entropy compositionally complex perovskite oxides

Dawei Zhang^a, Jiyun Park^b, Boyuan Xu^c, Cijie Liu^d, Wei Li^d, Xingbo Liu^d, Yue Qi^b, and Jian Luo^{a,e,#}

^a Program of Materials Science and Engineering, University of California San Diego, La Jolla, CA, 92093, USA

^b School of Engineering, Brown University, Providence, Rhode Island 02912, USA

^c Department of Physics, Brown University, Providence, Rhode Island 02912, USA

^d Department of Mechanical and Aerospace Engineering, Benjamin M. Statler College of Engineering and Mineral Resources, West Virginia University, Morgantown, WV 26506, USA

^e Department of NanoEngineering, University of California San Diego, La Jolla, CA, 92093, USA

Corresponding Author: jluo@alum.mit.edu

Section A: Method

1. Material synthesis and structural characterization

$(\text{La}_{1-x}\text{Sr}_x)(\text{Mn}_{1/3}\text{Fe}_{1/3}\text{Ti}_{1/3})\text{O}_3$ (LS_MFT) and $(\text{La}_{1-x}\text{Sr}_x)(\text{Mn}_{1/3}\text{Fe}_{1/3}\text{Cr}_{1/3})\text{O}_3$ (LS_MFC) were synthesized by conventional solid-state reaction methods. The sample compositions and abbreviations are shown in Table 1. Oxide precursors with specific stoichiometric amount of La_2O_3 (99.99%), SrCO_3 (99.9%), MnO_2 (99.5%), Fe_2O_3 (99.99%), TiO_2 (99.99%) and Cr_2O_3 (99.7%), purchased from Alfa Aesar, were weighted, and put into a high energy ball milling (HEBM) jar with 2 wt.% steric acid. The starting powder was ball milled for 100 min and then pressed into pellets with hydraulic press. The green body pellets were annealed under 1450 °C for 12 hours under air. After sintering, the pellets were crushed and grounded into powders, and subsequently re-pressed into new pellets for another 12 hours annealing process to improve the phase purity. Finally, the pellets (that formed pure phases) were crushed again into powder for further characterization.

The crystal structures of synthesized materials were examined by X-ray diffraction (XRD, Miniflex Rigaku, Japan) using $\text{Cu K}\alpha$ radiation, operating at 30 kV and 15 mA with a scan speed of 2°/min and a step size of 0.02°. The microstructure and elemental homogeneity were examined by scanning electron microscope (SEM, FEI Apero, OR, USA) with energy dispersive X-ray spectroscopy (EDS, Oxford N-Max^N) operating at 20 kV and 3.2 nA.

2. Temperature programmed reduction (TPR)

Temperature-programmed-reduction (TPR) experiments were conducted using a thermal gravimetric analyzer (TGA, Netzsch STA 449 F3 Jupiter). The mass of the samples used in these experiments was kept at around 30 mg. The temperature ramping profile was set to the following steps: (1) heating up at 25 °C/min to 1350 °C in UHP Ar and hold isothermally for 45 min; (2) cooling down to 900 °C while introducing 21% O_2 balanced with Ar for 25 min reoxidation; and (3) repeating Steps (1) and (2) for another cycle. The mass loss during the cycling was measured and the extent of reduction was calculated based on the following equation:

$$\delta = \frac{\Delta m * M_s}{m_s * M_o} \quad (1)$$

where δ is the extent of reduction, Δm stands for the mass loss measured by the TGA, M_s and M_O represent the molar mass of specimen and oxygen, respectively,

3. Electron energy loss spectroscopy (EELS)

EELS experiments were conducted using a ThermoFisher Talos 200X operating at 200 kV with EELS spectrometer (Continuum ER1065, Gatan). The EELS spectra were taken under the scanning transmission electron microscopy mode (STEM) with high-angle annular dark field (HAADF) detector. The imaging was performed with a 70 mrad collection angle. A dispersion of 0.2 eV per channel was used to collect all the energy edges including Ti-L_{2,3}, Cr-L_{2,3}, Mn-L_{2,3}, Fe-L_{2,3}, and O K edge. The background of core-loss EELS spectra (Mn, Fe, Ti, La and O) was fitted by power law in Gatan DigitalMicrograph 3 (GMS 3).

4. Density functional theory (DFT)

Density functional theory (DFT) calculations were performed to calculate the formation energy of a neutral oxygen vacancy. In order to avoid the interaction between oxygen vacancies, a 160-atom $2\sqrt{2} \times 2\sqrt{2} \times 2$ supercell of the orthorhombic LaBO₃ (B = Fe, Mn, Cr, and Ti) and SrCrO₃, and cubic SrBO₃ (B = Fe, Mn, and Ti) structures were used. All DFT calculations were performed using the Vienna Ab initio Simulation Package¹ with the generalized gradient approximation along with Perdew, Burke, and Ernzerhof (GGA-PBE)² and Hubbard U correction ($U_{eff} = 3, 3, \text{ and } 3.5$ eV for Fe, Mn, and Cr, respectively).^{3,4} The convergence criteria were 10^{-5} eV for the energy and 0.02 eV/Å for the atomic forces, and the planewave cutoff was set to 380 eV. The initial magnetic ordering was randomly half up and half down for the B-site cations, thus the total magnetic moment was set to zero. Since magnetic ordering of perovskites depends on temperature and pressure and the error associated with different magnetic configurations is the order of 0.01-0.02 eV/atom,⁵ only total magnetic moment was used as a constraint.^{6,7} The formation energy of a neutral oxygen vacancy was calculated as $E_V^f = E_{defective} - E_{bulk} + \mu_O^{FERE}$ where $E_{defective}$ and E_{bulk} indicate the DFT-calculated energy of a 160-atom supercell with and without a vacancy, respectively, and μ_O^{FERE} is the fitted elemental-phase reference energy (FERE) of oxygen (-4.76 eV for an oxygen atom).⁵ For orthorhombic structures, the smaller E_V^f between two different Wyckoff oxygen positions was chosen for the analysis.

Supplementary Figures:

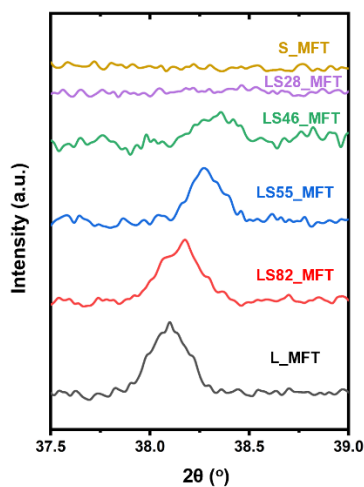


Figure S1. Enlarged views of the XRD patterns of the (113) peak area, showing the structural transition from rhombohedral $R\bar{3}c$ to cubic $Pm\bar{3}m$.

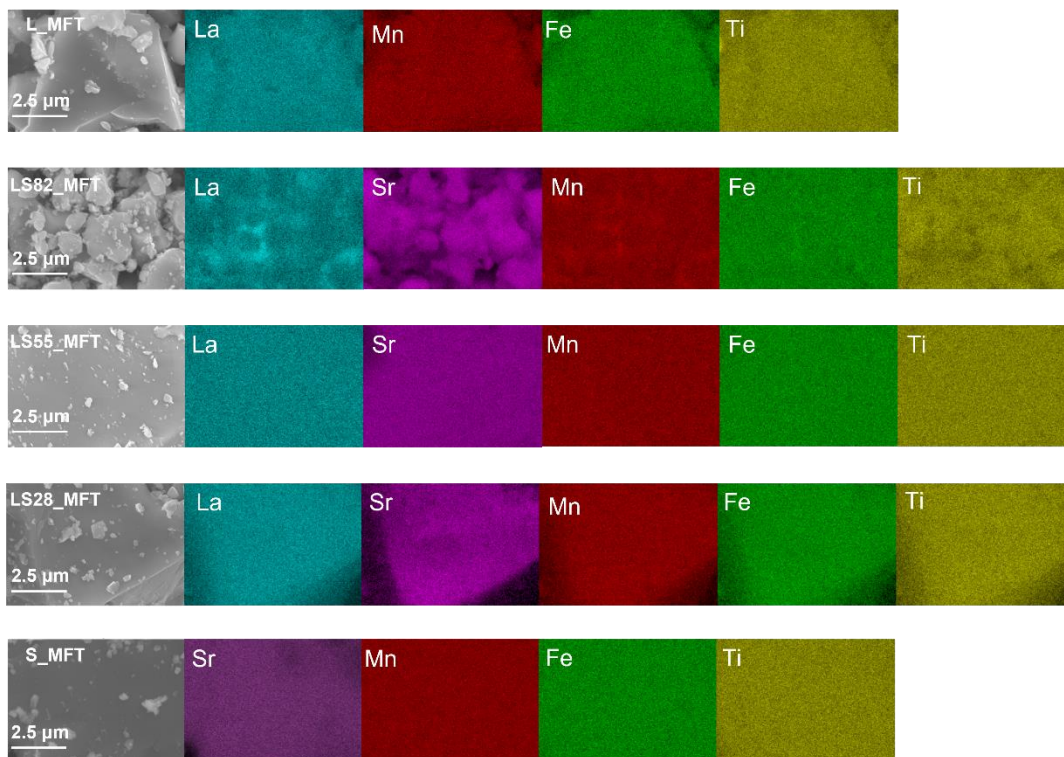


Figure S2. High-resolution SEM images and EDS elemental maps of five LS_MFT compositions, showing homogenous elemental distributions.

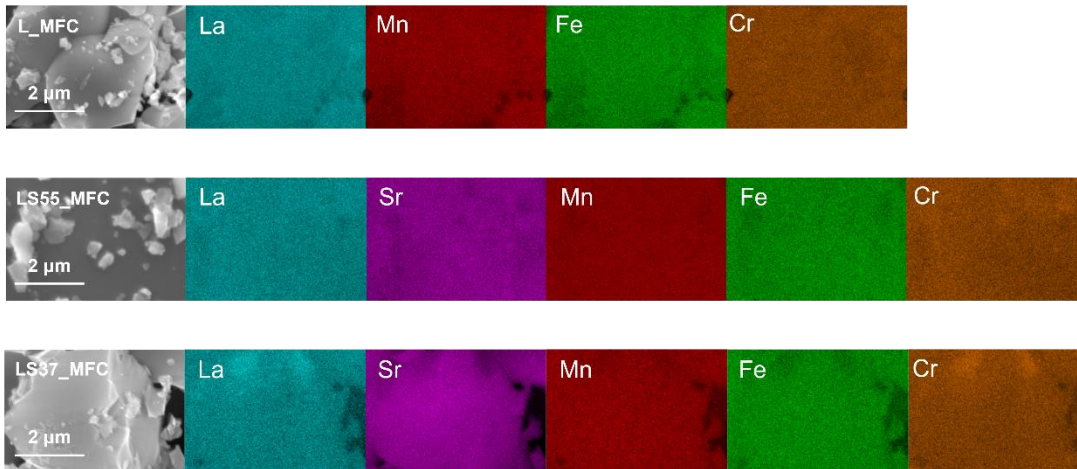


Figure S3. High-resolution SEM images and EDS element maps of three LS_MFC compositions.

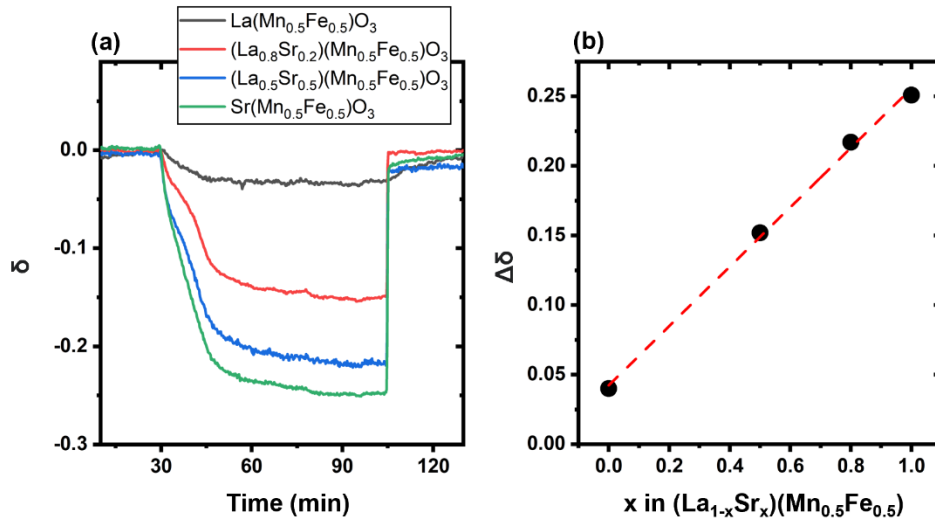


Figure S4. (a) Temperature programmed reduction measurements of $(\text{La}_{1-x}\text{Sr}_x)(\text{Mn}_{0.5}\text{Fe}_{0.5})\text{O}_3$. The reduction condition is at 1350 °C for 45 min under Ar. The oxidation was conducted at 900 °C for 25 min under 21% O_2 balanced with Ar. (b) The calculated $\Delta\delta$ vs. x in $(\text{La}_{1-x}\text{Sr}_x)(\text{Mn}_{0.5}\text{Fe}_{0.5})\text{O}_3$.

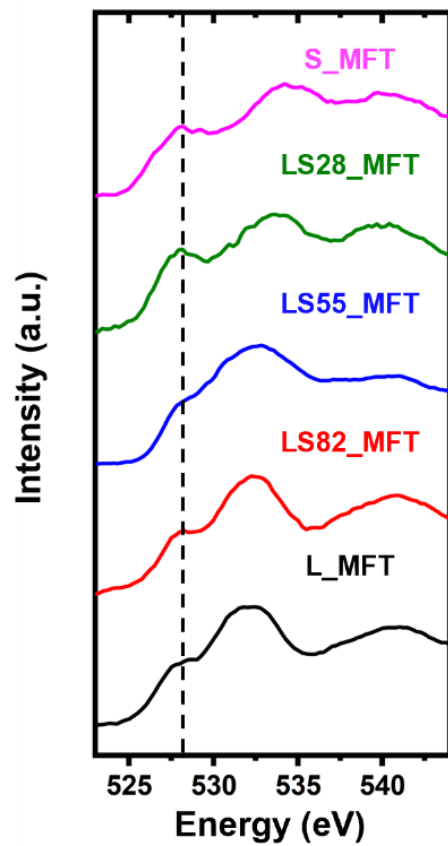


Figure S5. O K-edge EELS spectra of LS_MFT with varying Sr molar ratio.

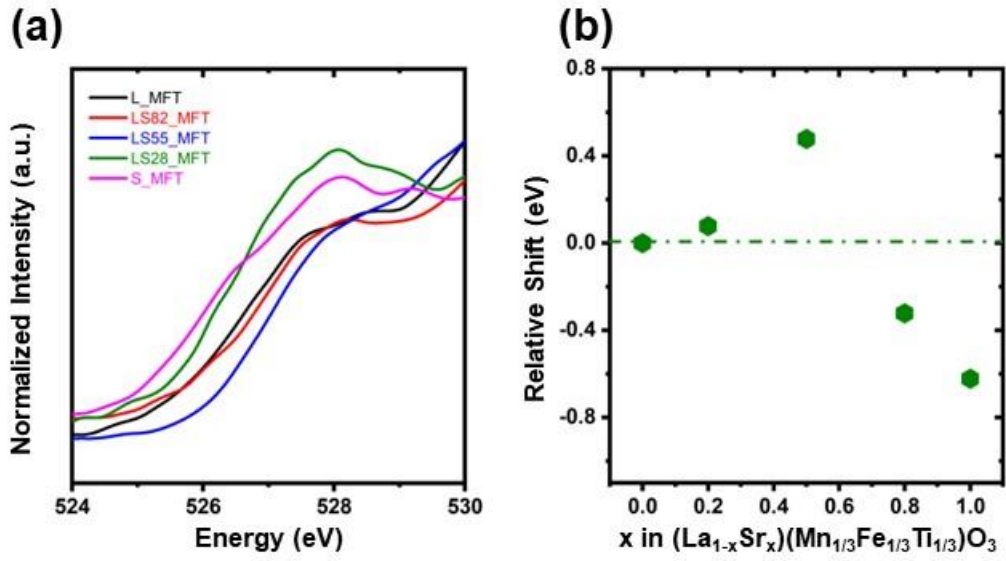


Figure S6. (a) O K edge onset of LS_MFT. (b) Calculated relative shift of the O K edge with different Sr molar ratios in the LS_MFT series.

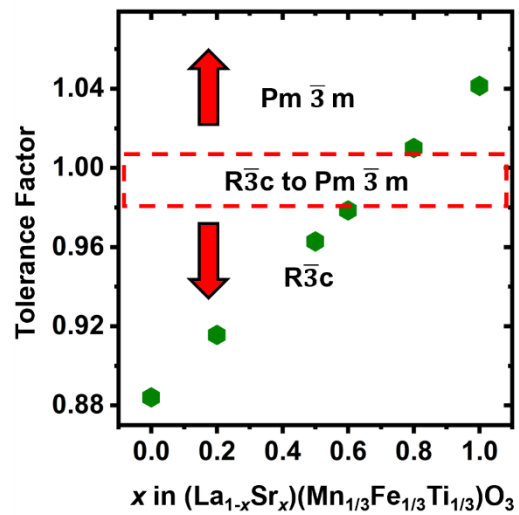


Figure S7. The Goldschmidt tolerance factor vs. x in $(La_{1-x}Sr_x)(Mn_{1/3}Fe_{1/3}Ti_{1/3})O_3$. The rhombohedral ($R\bar{3}c$) to cubic ($Pm\bar{3}m$) takes place when the Goldschmidt tolerance factor is close to 1.

References:

- 1 G. Kresse and J. Furthmüller, *Phys. Rev. B*, 1996, **54**, 11169.
- 2 J. P. Perdew, K. Burke and M. Ernzerhof, *Phys. Rev. Lett.*, 1996, **77**, 3865–3868.
- 3 T. Das, J. D. Nicholas and Y. Qi, *J. Mater. Chem. A*, 2017, **5**, 4493–4506.
- 4 A. A. Emery and C. Wolverton, *Sci. Data*, 2017, **4**, 170153.
- 5 V. Stevanović, S. Lany, X. Zhang and A. Zunger, *Phys. Rev. B - Condens. Matter Mater. Phys.*, 2012, **85**, 115104.
- 6 S. Tariq, A. A. Mubarak, B. Kanwal, F. Hamioud, Q. Afzal and S. Zahra, *Chinese J. Phys.*, 2020, **63**, 84–91.
- 7 M. T. Curnan and J. R. Kitchin, *J. Phys. Chem. C*, 2014, **118**, 28776–28790.